IOPscience iopscience.iop.org

Home Search Collections Journals About Contact us My IOPscience

Anisotropic intermediate coupling superconductivity in $Cu_{0.03}TaS_2$

This article has been downloaded from IOPscience. Please scroll down to see the full text article.

2009 J. Phys.: Condens. Matter 21 145701

(http://iopscience.iop.org/0953-8984/21/14/145701)

View the table of contents for this issue, or go to the journal homepage for more

Download details:
IP Address: 202.127.206.173
The article was downloaded on 17/07/2012 at 02:50

Please note that terms and conditions apply.

J. Phys.: Condens. Matter **21** (2009) 145701 (6pp) doi:10.1088/0953-8984/21/14/145701

Anisotropic intermediate coupling superconductivity in $Cu_{0.03}TaS_2$

Xiangde Zhu[1], Yuping Sun[1,2], Shuhua Zhang[1], Jianglong Wang[3], Liangjian Zou[1], Lance E DeLong[4], Xuebin Zhu[1], Xuan Luo[1], Bosen Wang[1], Gang Li[1], Zhaorong Yang[1] and Wenhai Song[1]

[1] Key Laboratory of Materials Physics, Institute of Solid State Physics, Chinese Academy of Sciences, Hefei 230031, People's Republic of China
[2] High Magnetic Field Laboratory, Chinese Academy of Sciences, Hefei 230031, People's Republic of China
[3] College of Physics Science and Technology, Hebei University, Baoding 071002, People's Republic of China
[4] Department of Physics and Astronomy, University of Kentucky, Lexington, KY 40506-0055, USA

E-mail: ypsun@issp.ac.cn and zou@theory.issp.ac.cn

Received 15 December 2008, in final form 12 February 2009
Published 5 March 2009
Online at stacks.iop.org/JPhysCM/21/145701

Abstract
The anisotropic superconducting state properties in $Cu_{0.03}TaS_2$ have been investigated by magnetization, magnetoresistance and specific heat measurements. They clearly show that $Cu_{0.03}TaS_2$ undergoes a superconducting transition at $T_C = 4.03$ K. The obtained superconducting parameters demonstrate that $Cu_{0.03}TaS_2$ is an anisotropic type-II superconductor. Combining specific heat jump $\Delta C/\gamma_n T_C = 1.6(4)$, gap ratio $2\Delta/k_B T_C = 4.0(9)$ and the estimated electron–phonon coupling constant $\lambda \sim 0.68$, the superconductivity in $Cu_{0.03}TaS_2$ is explained within the intermediate coupling BCS scenario. First-principles electronic structure calculations suggest that copper intercalation of 2H-TaS_2 causes a considerable increase of the Fermi surface volume and the carrier density, which suppresses the CDW fluctuation and favors the raise of T_C.

(Some figures in this article are in colour only in the electronic version)

1. Introduction

The compounds 2H-TaS_2, 2H-$TaSe_2$ and 1T-TiS_2 are layered transition-metal dichalcogenides (TMDC) [1, 2], formed by stacking covalently bonded X–T–X layers that are weakly coupled by van der Waals bonding. Additional atoms and organic molecules can be inserted into the gap between the layers, forming intercalated compounds. Since the discoveries of superconductivity in potassium intercalated graphite KC_8 in 1965 [3] and $(Py)_{1/2}TaS_2$ in 1970 [4], superconductivity induced by intercalation has been widely investigated in highly oriented pyrolitic graphite (HOPG) [5] and layered TMDC [6]. The recent discoveries of superconductivity in CaC_6 with $T_C = 11.5$ K [7] and the suppression of charge density wave (CDW) order in Na_xTaS_2 [8] and Cu_xTiSe_2 [9] have renewed interest in intercalated layered compounds. To date, the influence of transition-metal intercalation on electronic structure is still not clear. For example, a rigid band model with charge transfer was proposed by assuming that intercalation only alters the density of state (DOS) at the Fermi level (E_F) without any other change in the electronic structure [10]. However, previous experiments in intercalated graphite compounds did not support the rigid band model [11]. It is therefore of interest to determine if the rigid band model is applicable to TMDC, which is a question not yet answered in the literature.

2H-TaS_2 is a typical layered TMDC that exhibits coexisting CDW (TCDW $\sim$ 78 K) and superconducting ($T_C \sim$ 0.8 K) phases [12]. Enhanced superconductivities have been discovered in many organic molecules intercalated 2H-TaS_2 [4, 13, 14], alkali metal intercalated A_xTaS_2 [15] and 3D transition metal Fe dilute intercalated 2H-$Fe_{0.05}TaS_2$ [16]. Recently, the basic superconducting properties of the polycrystalline Cu_xTaS_2 have been reported by the Cava group [17]. However, the anisotropic superconducting state parameters have not been characterized yet, and the origin of the T_C enhancement by copper intercalation is

 © 2009 IOP Publishing Ltd Printed in the UK

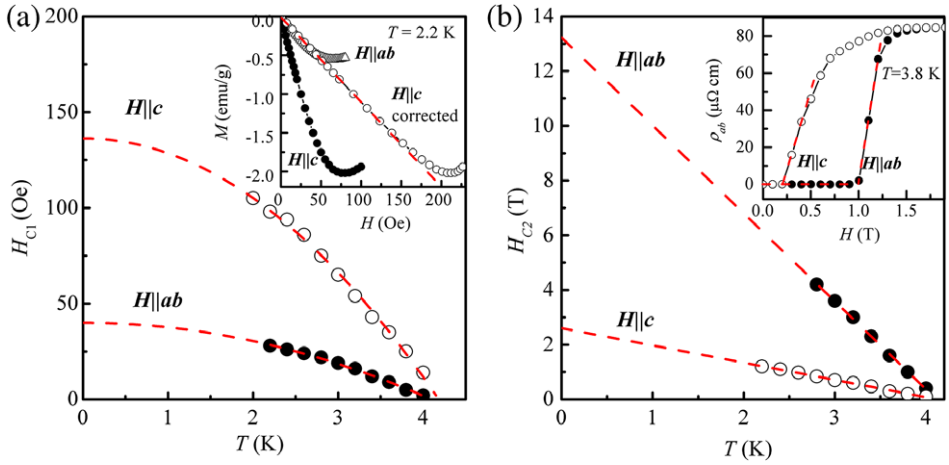

Figure 1. (a) Temperature (T) dependence of the lower critical field (H_{C1}) for $Cu_{0.03}TaS_2$. The dashed line shows the fitted curve. The inset shows the magnetization as a function of applied field (M–H curves) measured at $T = 2.2$ K, for $\boldsymbol{H} \parallel \boldsymbol{ab}$, $\boldsymbol{H} \parallel \boldsymbol{c}$ and $\boldsymbol{H} \parallel \boldsymbol{c}$ with demagnetization effect correction. (b) Temperature dependence of the upper critical field (H_{C2}) for $Cu_{0.03}TaS_2$. The dashed line shows the fitted linear curve. The inset shows in-plane resistivity (ρ_{ab}) as a function of applied field both for $\boldsymbol{H} \parallel \boldsymbol{ab}$ and $\boldsymbol{H} \parallel \boldsymbol{c}$ measured at $T = 3.8$ K.

still unknown. In this paper, we present the anisotropic superconducting properties of $Cu_{0.03}TaS_2$ single crystal and comprehensively analyze the superconductivity in $Cu_{0.03}TaS_2$ within the intermediate coupling BCS scenario. We perform first-principles electronic structure calculations based on the tight-binding linear muffin-tin orbital (TB-LMTO) approach, suggesting that the substantial increase of T_C in $Cu_{0.03}TaS_2$ originates from the enlargement of the Fermi surface volume and the increase of carrier density with copper intercalation, and that the significant alteration of the band structures near E_F invalidates the rigid band approximation.

2. Experimental details

Dilute copper intercalates of composition Cu_xTaS_2 ($x = 0.03$) were grown as single crystals via chemical vapor transport with iodine as a transport agent [18]. The magnetization (M) measurements were performed with a SQUID magnetometer (Quantum Design MPMS). The specific heat (C) and the magnetoresistance measurements were carried out with a physical property measurement system (Quantum Design PPMS).

The microscopic electronic states and possible origin of the profound increase in the superconducting temperature in Cu_xTaS_2 were investigated by the first-principles electronic structure calculations, utilizing the tight-binding linear muffin-tin orbitals within the atomic sphere approximation (TB-LMTO-ASA) scheme for the supercells of $2 \times 2 \times 1$ and $2 \times 2 \times 2$, corresponding to Cu concentrations of $x = 1/8$ and $1/16$.

3. Experimental results and analysis

3.1. Anisotropic superconducting parameters

Figure 1(a) shows the temperature dependence of the lower critical field H_{C1} for $\boldsymbol{H} \parallel \boldsymbol{ab}$ and $\boldsymbol{H} \parallel \boldsymbol{c}$ (after demagnetization correction) determined from the measured M–H curves. The temperature dependence of $H^i_{C1}(T)$ (where i donates the field applied along the i direction) can be well fitted to $H^i_{C1}(T) = H^i_{C1}(0)[1 - (T/T_C)^2]$ [19]. The inset of figure 1(a) shows the typical field dependence of M–H curves measured at $T = 2.2$ K. Due to the plate shape of the single-crystal sample, the demagnetization effect for $\boldsymbol{H} \parallel \boldsymbol{ab}$ is negligible, while the demagnetization for $\boldsymbol{H} \parallel \boldsymbol{c}$ is large. Demagnetization corrections of the M–H curves for $\boldsymbol{H} \parallel \boldsymbol{c}$ were performed according to [20]. For comparison, the corrected M–H curve for $\boldsymbol{H} \parallel \boldsymbol{c}$ is also shown in the inset of figure 1(a).

The upper critical field H_{C2} can be obtained from the in-plane magnetoresistance measurements (ρ_{ab}–H) for $\boldsymbol{H} \parallel \boldsymbol{ab}$ and $\boldsymbol{H} \parallel \boldsymbol{c}$. Figure 1(b) shows the typical temperature dependences of the upper critical field (H_{C2}) for $\boldsymbol{H} \parallel \boldsymbol{ab}$ and $\boldsymbol{H} \parallel \boldsymbol{c}$, and the inset of figure 1(b) depicts $\rho_{ab} - H$ curves for $\boldsymbol{H} \parallel \boldsymbol{ab}$ and $\boldsymbol{H} \parallel \boldsymbol{c}$ at $T = 3.8$ K. The $H_{C2}(T)$ data exhibit an almost linear temperature dependence near T_C, which is consistent with the Werthamer–Helfand–Hohenberg (WHH) model for type-II superconductors [21]. Extrapolations of $H_{C2}(0)$ were performed with the WHH equation

$$H_{C2}(0) = 0.693[-(\mathrm{d}H_{C2}/\mathrm{d}T)]_{T_C} T_C.$$

The determined $H_{C1}(0)$ and $H_{C2}(0)$ are: $H^{ab}_{C1}(0) \approx 40$ Oe, $H^{c}_{C1}(0) \approx 135$ Oe, $H^{ab}_{C2}(0) \approx 9.16$ T and $H^{c}_{C2}(0) \approx 1.8$ T.

According to the H_{C2}–T relations in figure 1(b), the Ginzburg–Landau (GL) anisotropy parameter, $\gamma_{anis} = H^{ab}_{C2}/H^{c}_{C2} = 5.1$, is roughly temperature-independent. with the GL formulae for anisotropic upper critical fields: $H^{ab}_{C2}(0) = \Phi_0/(2\pi\xi_{ab}\xi_c)$ and $H^{c}_{C2}(0) = \Phi_0/(2\pi\xi^2_{ab})$, where Φ_0 is the flux quantum and the GL coherence lengths are estimated to be $\xi_{ab} = 13.5$ nm and $\xi_c = 2.65$ nm, respectively. The GL parameters $\kappa_i(0)$ are also obtained with the equation $H^i_{C2}(0)/H^i_{C1}(0) = 2\kappa^2_i(0)/\ln\kappa_i(0)$. With $H_C(0) = H^{ab}_{C1}(0)/\sqrt{2}\kappa_{ab}(0)$, the thermodynamic critical field $H_C(0)$ is determined to be $\approx$0.1 T. The GL penetration length is evaluated through $\kappa_c(0) = \lambda_{ab}(0)/\xi_{ab}(0)$ and $\kappa_{ab}(0) = \lambda_{ab}(0)/\xi_c(0) = [\lambda_{ab}(0)\lambda_c(0)/\xi_{ab}(0)\xi_c(0)]^{1/2}$. We note that

Table 1. Superconducting parameters for $Cu_{0.03}TaS_2$: critical temperature for superconductivity T_C, Sommerfeld coefficient γ_n, Debye temperature Θ_D, electron–phonon coupling constant λ, specific heat jump $\Delta C/\gamma_n T_C$, gap ratio $2\Delta/k_B T_C$, upper critical field $H_{C2}(0)$, lower critical field $H_{C1}(0)$ (after demagnetization correction), thermodynamic critical field $H_C(0)$, GL parameters $\kappa(0)$, GL coherence length $\xi_{GL}(0)$, GL penetration depth $\lambda(0)$ and GL anisotropy ratio of $H_{C2}\gamma_{anis}$.

Superconducting state parameters for $Cu_{0.03}TaS_2$			
		$H \parallel ab$	$H \parallel c$
T_C (K)	4.03		
γ_n (mJ mol^{-1} K^{-2})	10.8(5)		
Θ_D (K)	246		
λ	0.68		
$\Delta C/\gamma_n T_C$	1.64		
$2\Delta/k_B T_C$	4.09		
$H_{C2}(0)$ (T)		9.16	1.8
$H_{C1}(0)$ (Oe)		40	135
$H_C(0)$ (T)	~0.1		
κ (0)		69.7	13.1
ξ_{GL} (0)		13.5	2.65
λ (0) (nm)		177	983
γ_{anis}	5.1		

the obtained superconducting parameters can be approximately fitted to the anisotropic GL relation:

$$\gamma_{anis} = \frac{H_{C2}^{ab}}{H_{C2}^{c}} = \frac{\xi_{ab}}{\xi_c} = \frac{\lambda_c}{\lambda_{ab}} = \frac{\kappa_{ab}}{\kappa_c} \sim \frac{H_{C1}^{c}}{H_{C1}^{ab}}.$$

All these parameters are summarized in table 1 and they indicate that $Cu_{0.03}TaS_2$ is a typical type-II superconductor with a large anisotropy.

3.2. Specific results and discussions

Data for the specific heat divided by temperature, C/T, for $Cu_{0.03}TaS_2$ are shown in figure 2 as a function of T^2 with magnetic fields $H = 0$ and 2.5 kOe applied perpendicular to the ab plane. The sharp jump in the specific heat data at $T_C = 4.03$ K indicates the bulk nature of superconductivity and the high quality of our $Cu_{0.03}TaS_2$ samples, which is corroborated by a sharp drop of the magnetic susceptibility (shown in the inset of figure 2) at $T = 4.2$ K with a transition width (10%–90%) of 0.2 K and a zero-field-cooling (ZFC) curve that indicates a perfect shielding effect.

The low temperature specific heat C in the normal state can be usually described by $C = C_e + C_l$, where $C_e = \gamma_n T$ is the electronic contribution and $C_l(T) = \beta T^3 + \delta T^5$ is the lattice contribution. The dashed curve in figure 2 is the best fitting of the data to this model for $H = 0$ Oe and $T \leqslant 10$ K, yielding the parameters $\gamma_n = 10.8(5)$ mJ mol^{-1} K^{-2}, $\beta = 0.39(3)$ mJ mol^{-1} K^{-4} (corresponding Debye temperature $\Theta_D = 246$ K) and $\delta = 0.2(3)$ μJ mol^{-1} K^{-6}. Compared with the matrix 2H-TaS_2 with $\gamma_n = 8.5$ mJ mol^{-1} K^{-2} and $\beta = 0.37$ mJ mol^{-1} K^{-4} (shown in table 2) [22], the value of γ_n for $Cu_{0.03}TaS_2$ is slightly larger, while the value of β is almost the same.

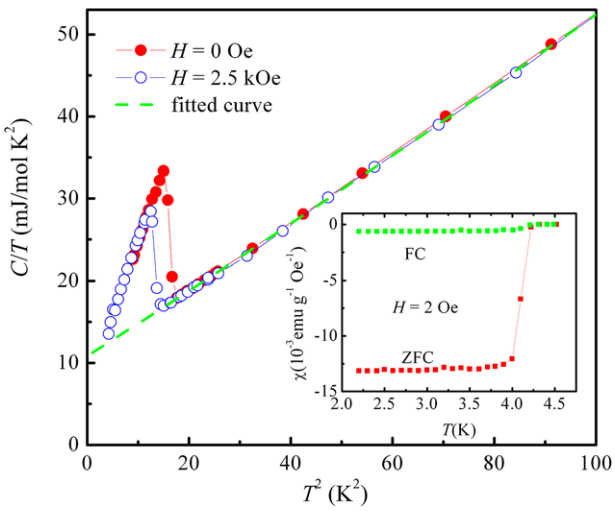

Figure 2. Specific heat divided by temperature (C/T) as a function of T^2 for $Cu_{0.03}TaS_2$ measured at $H = 0$ (solid circles, ●) and $H = 2.5$ kOe (open circles, ○). The dashed line represents the best-fit curve. The inset shows the temperature dependence of the dc magnetic susceptibilities with $H = 2$ Oe applied parallel to ab plane under zero-field-cooled (ZFC) and field-cooled (FC) conditions.

Table 2. The superconducting transition temperature (T_C) and specific heat parameters for $Cu_{0.03}TaS_2$, compared with those of 2H-TaS_2, $Py_{1/2}TaS_2$, 2H-$NbSe_2$ and Cu_xTiSe_2.

Compound	T_C (K)	γ_n (mJ mol^{-1} K^{-2})	β (mJ mol^{-1} K^{-4})	$\Delta C/\gamma_n T_C$	Ref.
$Cu_{0.03}TaS_2$	4.03	10.8(5)	0.39(3)	1.64	This work
2H-TaS_2	0.8	8.5	0.37	1.9	[17]
$Py_{1/2}TaS_2$	3.5	9.1	2.32	0.96	[17]
2H-$NbSe_2$	7.1	16.5	0.53	1.73	[17]
Cu_xTiSe_2	4.1	4.3	...	1.68	[8]

With the McMillan formula [23]

$$\lambda = \frac{\mu^* \ln(\frac{1.45T_C}{\Theta_D}) - 1.04}{1.04 + \ln(\frac{1.45T_C}{\Theta_D})(1 - 0.62\mu^*)},$$

the electron–phonon coupling constant λ is estimated to be ~0.68 by assuming the Coulomb pseudopotential $\mu^* = 0.15$, which is a typical value of an intermediate coupling BCS superconductor.

The temperature dependence of the C_e/T for $H = 0$ Oe near the superconducting transition is shown in figure 3. From the obtained ln $(C_e/\gamma_n T_C)$ versus T_C/T data shown in the inset of figure 3, the ratio of the gap and the critical temperature is about, $2\Delta/k_B T_C = 4.09$, significantly larger than the BCS value (3.53) in the weak coupling limit [19]. The dashed curve depicted in figure 3 is the theoretical result of the isotropic s-wave BCS gap with $2\Delta/k_B T_C = 4.09$, in good agreement with the experimental data. The extracted specific heat jump at T_C, $\Delta C/\gamma_n T_C = 1.64$, is also significantly larger than the weak coupling value 1.43, implying intermediate coupling [23]. This value is similar to $\Delta C/\gamma_n T_C = 1.68$ observed for another dilute TMDC, Cu_xTiSe_2 [9], although it is markedly less than the observed values of 1.9 in 2H-TaS_2 and 2.1 in

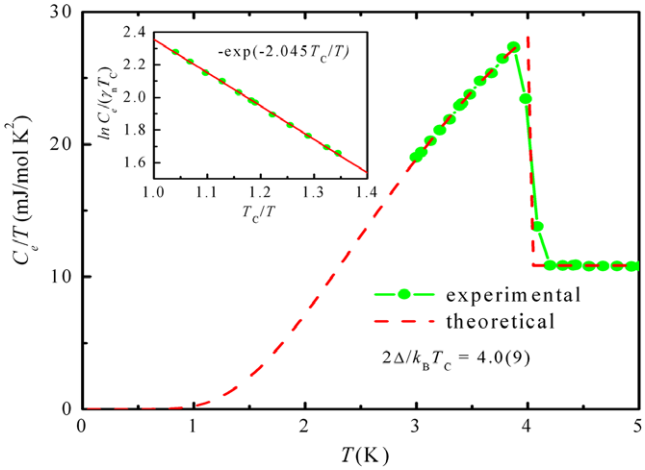

Figure 3. Temperature dependence of the electronic specific heat divided by temperature, C_e/T at $H = 0$ Oe for $Cu_{0.03}TaS_2$. The solid line shows C_e/T calculated by assuming an isotropic s-wave BCS gap with $2\Delta/k_BT_C = 4.09$.

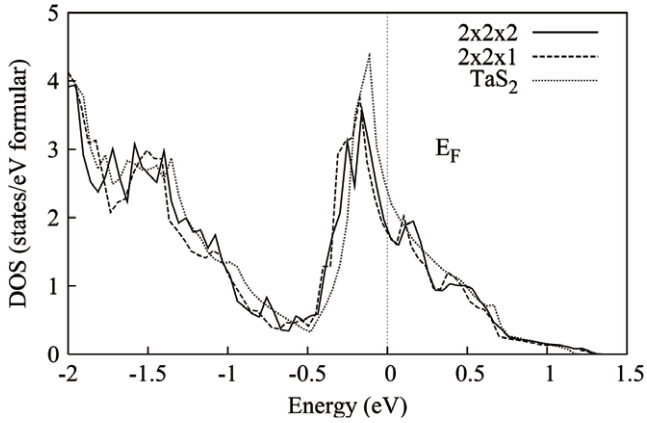

Figure 4. The density of states (DOS) in Cu_xTaS_2 in normal state for the supercell $2 \times 2 \times 2$ (solid line) and the supercell $2 \times 2 \times 1$ (dashed line). The DOS of undoped 2H-TaS_2 is also plotted for comparison (dotted line).

2H-$NbSe_2$ [22]. All the determined parameters of the specific heat compared with 2H-TaS_2, 2H-$NbSe_2$ and Cu_xTiSe_2 are listed in table 2.

3.3. Calculation and discussions

According to the experimental x-ray diffraction data, the lattice constants a and c of Cu_xTaS_2 are expanded from those of TaS_2, $a = 0.3310$ to 0.3312 nm and $c = 1.2080$ to 1.2137 nm, strongly suggesting that Cu is intercalated into the van der Waals gap. In our calculation, the Cu position is assumed to be located at the fractional coordinate $(0, 0, 1/2)$. The DOS near E_F of Cu_xTaS_2 at $x = 0, 1/16$ and $1/8$ is shown in figure 4. It is found that the Fermi energy of 2H-TaS_2 is very close to a sharp DOS peak, in agreement with the earlier results [24]. This also resembles the DOS in CDW Cu_xTiSe_2 [25], indicating that these compounds lie at the edge of a spatial charge modulating phase. Thus 2H-TaS_2 is unstable with respect to the transition into the CDW phase. In the homogeneous 2H-TaS_2, the theoretical DOS near the E_F, $N(0)$, is about 1.2 states/eV-cell-spin. After Cu intercalation, the theoretical $N(0)$ for Cu_xTaS_2 at $x = 1/16$ is about 1.0 states/eV-cell-spin, which is slightly smaller than that in 2H-TaS_2. The slight decrease in $N(0)$ originates from the fact that the Cu intercalation brings more carriers, leading to the increase in E_F and the Fermi energy shifts right from the DOS peak, as shown in figure 4. Meanwhile, the carriers from copper enlarge the volume of the Fermi surface through entering the CDW gap, as seen in figure 4. We notice that the increase of the Fermi energy was also found in CDW and superconducting Cu_xTiSe_2 [26]. Thus in Cu_xTaS_2, on the one hand, the Cu intercalation brings more and more carriers into the Fermi surface and reduces the CDW gap, as we experimentally find that the CDW transition temperature decreases from 78 K in 2H-TaS_2 to 50 K in $Cu_{0.03}TaS_2$ [18]; on the other hand, more carriers can participate in the superconducting pairing and raise the T_C. Therefore, Cu-intercalated TaS_2 suppress the CDW instability, favoring the superconductivity in Cu_xTaS_2.

From figure 4, we also found that the single DOS peak in 2H-TaS_2 splits into two peaks in Cu_xTaS_2, implying that the rigid band model [10] is not a good approximation for describing the evolution of the electronic structures upon Cu doping. Meanwhile, we plot the TB-LMTO band structures of Cu_xTaS_2 for the $2 \times 2 \times 2$ supercell. The energy band structure near E_F considerably changes upon intercalation, as shown in figure 5. Compared to the electronic structures of 2H-TaS_2 [24], though Cu 3d bands lie below E_F, a fraction of Cu 4s electrons participate in the Fermi surface, leading to obvious changes in the band structure near E_F in Cu_xTaS_2. The considerable variations in the DOS, the electronic structures and the existence of an optimal doping in superconducting Cu_xTaS_2 [18] demonstrate that the rigid band model is invalid in Cu-intercalated TaS_2.

In layered superconducting TMDC, the relationship among the electron–phonon coupling, the superconductivity and the CDW order has been explored for many years and is still under debate. As we see in figures 4 and 5, the Cu 4s electrons gained via Cu intercalation fill in the CDW gap and suppress CDW order; this leads Cu_xTaS_2 to transit from the CDW phase to the superconducting phase. Recently, Cava *et al* [9] reported that Cu-intercalated Cu_xTiSe_2 also undergoes a transition from CDW order to a superconducting phase; the properties of Cu_xTiSe_2 in the CDW and the superconducting phases are very similar to the behavior we observe here for Cu-doped TaS_2, including the considerable increase in E_F with Cu doping. On the other hand, other authors [27–29] showed that, in TiS_2, neither does there exist the CDW order, nor does Cu doping induce a superconducting transition, though the processes of sample preparation are identical to those for Cu_xTaS_2. From these results, one may find a close relationship between the CDW order and the superconductivity in TMDC: strong electron–phonon coupling not only promotes a CDW ground state, but also drives superconducting pairing in layered TMDC. In contrast, the electron–phonon coupling in TiS_2 is

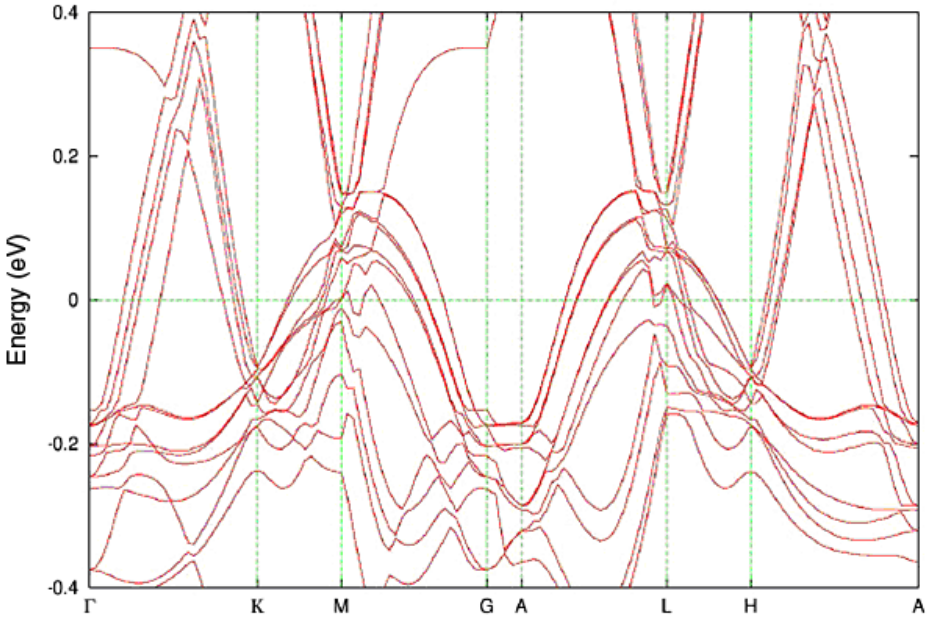

Figure 5. The energy band structures of Cu_xTaS_2 by the TB-LMTO-ASA method for the supercell $2 \times 2 \times 2$, corresponding to Cu concentration $x = 1/16$. Details of the electronic structure of undoped 2H-TaS_2 can be found in [24] for comparison.

so weak that neither CDW order nor superconductivity can form [28, 29].

4. Conclusion

In summary, the electronic structure and anisotropic superconducting state parameters of $Cu_{0.03}TaS_2$ have been determined. The GL anisotropy, the specific heat jump, the gap ratio and the electron–phonon coupling definitely show that $Cu_{0.03}TaS_2$ is an anisotropic, intermediate coupling, type-II BCS superconductor. First-principles electronic structure calculations suggest that copper intercalation of 2H-TaS_2 causes a considerable increase of the Fermi surface volume and the carrier density, which suppresses the CDW fluctuations and favors the rise of T_C.

Acknowledgments

This work was supported by the National Key Basic Research under contract nos. 2006CB601005 and 2007CB925002, the National Nature Science Foundation of China under contract nos, 10774146 and 10774147, the Bairen Project, and the Director's Fund of Hefei Institutes of Physical Science, Chinese Academy of Sciences. Research at the University of Kentucky was supported by the US Dept. of Energy grant no. DE-FG02-97ER45653 and the US National Science Foundation grant nos. DMR-0240813 and DMR-0552267.

References

[1] Wilson J A and Yoffe A D 1969 *Adv. Phys.* **18** 193
[2] Wilson J A, Di Salvo F J and Mahajan S 1975 *Adv. Phys.* **24** 117
[3] Hannay N B, Geballe T H, Matthias B T, Andres K, Schmidt P and MacNair D 1965 *Phys. Rev. Lett.* **14** 225
[4] Gamble F R, Di Salvo F J, Klemm R A and Geballe T H 1970 *Science* **168** 568
[5] Dresselhaus M S and Dresselhaus G 2002 *Adv. Phys.* **51** 1
[6] Friend R H and Yoffe A D 1987 *Adv. Phys.* **36** 1
[7] Weller T E, Ellerby M, Saxena S S, Smith R P and Skipper N T 2005 *Nat. Phys.* **1** 39
[8] Fang L, Wang Y, Zou P Y, Tang L, Xu Z, Chen H, Dong C, Shan L and Wen H H 2005 *Phys. Rev.* B **72** 014534
[9] Morosan E, Zandbergen H W, Dennis B S, Bos J W G, Onose Y, Klimczuk T, Ramirez A P, Ong N P and Cava R J 2006 *Nat. Phys.* **2** 544 and references therein
[10] McCanny J V 1979 *J. Phys. C: Solid State Phys.* **12** 3283
[11] Eberhardt W, McGovern I T, Plummer E W and Fisher J E 1980 *Phys. Rev. Lett.* **44** 200
[12] Harper J M E, Geballe T H and Di Salvo F J 1977 *Phys. Rev.* B **15** 2943
[13] Meyer S F, Howard R E, Stewart G R, Acrivos J V and Geballe T H 1975 *J. Chem. Phys.* **62** 4411
[14] Schlicht A, Lerf A and Biberacher W 1999 *Synth. Met.* **102** 1483
[15] Lerf A, Sernetz F, Biberacher W and Schöllhorn R 1979 *Mater. Res. Bull.* **14** 797
[16] Fleming R M and Coleman R V 1975 *Phys. Rev. Lett.* **34** 1502
[17] Wagner K E, Morosan E, Hor Y S, Tao J, Zhu Y, Sanders T, McQueen T M, Zandbergen H W, Williams A J, West D V and Cava R J 2008 *Phys. Rev.* B **78** 104520
[18] Zhu X D, Sun Y P, Zhu X B, Luo X, Wang B S, Li G, Yang Z R, Song W H and Dai J M 2008 *J. Cryst. Growth* **311** 218
[19] Bardeen J, Cooper L N and Schrieffer J R 1957 *Phys. Rev.* **108** 1175
[20] Kunchur M N and Poon S J 1991 *Phys. Rev.* B **43** 2916
[21] Werthamer N R, Helfand E and Hohenberg P C 1966 *Phys. Rev.* **147** 295
[22] Meyer S F, Howard R E, Stewart G R, Acrivos J V and Geballe T H 1975 *J. Chem. Phys.* **62** 4411
[23] McMillan W L 1968 *Phys. Rev.* **167** 331

[24] Guo G Y and Liang W Y 1987 *J. Phys. C: Solid State Phys.* **20** 4315
[25] Jeong T and Jarlborg T 2007 *Phys. Rev.* B **76** 153103
[26] Zhao J F, Ou H W, Wu G, Xie B P, Zhang Y, Shen D W, Wei J, Yang L X, Dong J K, Arita M, Namatame H, Taniguchi M, Chen X H and Feng D L 2007 *Phys. Rev. Lett.* **99** 146401
[27] Tazuke Y, Kuwazawa K, Onishi Y and Hashimoto T 1991 *J. Phys. Soc. Japan* **60** 2534
[28] Kusawake T, Takahashi Y, Ohshima K and Wey M Y 1999 *J. Phys.: Condens. Matter* **11** 6121
[29] Kusawake T, Takahashi Y, Wey M Y and Ohshima K 2001 *J. Phys.: Condens. Matter* **13** 9913